Editors' Suggestion | Featured in Physics

3D Strain in 2D Materials: To What Extent is Monolayer Graphene Graphite?

Y. W. Sun,[1,*] W. Liu,[2] I. Hernandez,[3] J. Gonzalez,[3] F. Rodriguez,[3] D. J. Dunstan,[4,†] and C. J. Humphreys[1,‡]
[1]School of Engineering and Materials Science, Queen Mary University of London, London E1 4NS, United Kingdom
[2]College of Information Science and Electronic Engineering, Zhejiang University, Hangzhou 310027, China
[3]Departamento CITIMAC, Universidad de Cantabria, Santander 39005, Spain
[4]School of Physics and Astronomy, Queen Mary University of London, London E1 4NS, United Kingdom

(Received 5 April 2019; revised manuscript received 28 May 2019; published 25 September 2019)

This work addresses a fundamental question: To what extent is graphene graphite? In particular does 2D graphene have many of the same 3D mechanical properties as graphite, such as the bulk modulus and elastic constant c_{33}? We have obtained, for the first time, unambiguous Raman spectra from unsupported monolayer graphene under pressure. We have used these data to quantify the out-of-plane stiffness of monolayer graphene, which is hard to define due to its 2D nature. Our data indicate a first physically meaningful out-of-plane stiffness of monolayer graphene, and find it to be consistent with that of graphite. We also report a shift rate of the in-plane phonon frequency of unsupported monolayer graphene to be 5.4 $cm^{-1}\,GPa^{-1}$, very close to that of graphite (4.7 $cm^{-1}\,GPa^{-1}$), contrary to the previous value for supported graphene. Our results imply that monolayer graphene has similar in-plane and out-of-plane stiffnesses, and anharmonicities to graphite.

DOI: 10.1103/PhysRevLett.123.135501

Monolayer materials such as graphene are often described as 2D materials, and indeed their 2D nature has profound dimensionality effects [1–3]. Yet they are often modeled as sheets of isotropic 3D material with a very small effective thickness, even as low as 0.066 nm [4,5]. We show here that the true thickness of graphene (due to the π electrons above and below the hexagonal network of sp^2 bonded carbon atoms) and its 3D elastic stiffness tensor does retain meaning, corresponding to real experimental observables, in particular that it makes sense to ascribe a 3D strain tensor to monolayer graphene.

Graphene has many extraordinary properties due to its 2D nature. It also brings challenges. For example, a continuum 3D model cannot be applied to graphene to obtain its elasticity. Strain is usually defined by the displacement of atomic core. Their positions are easily measured to quantify deformation (strain). There is no such displacement for monolayer graphene along the c axis. Without an explicit and meaningful definition of 3D strain, 3D elasticity, in particular the out-of-plane stiffness (or the elastic constant c_{33}), of graphene cannot be obtained. Consequently, the response of graphene (2D) to pressure (3D) cannot be described conventionally.

However, it is the electron orbitals that experience and react to strain. For example, in diamond under deformation, it is the sp^3 orbitals that experience and resist changes of angles and lengths. In graphite in compression, it is the p orbitals that are compressed, and that resist this compression. It is therefore reasonable to extend this concept to monolayer graphene, to allow the electron orbitals a certain spatial extent in equilibrium, and to recognize that they will resist confinement to a reduced spatial extent. This translates into a c_{33} defined by the resistance of the p orbitals to compression. In this way, graphene can have as meaningful a set of 3D elastic parameters as, say, MoS_2, where there are atomic nuclei to inform us about the deformations in the electron orbitals in the c-axis direction.

Investigating the mechanical properties of graphene is essential both for fundamental understanding and for the development of novel graphene-based nanostructures [6] and devices [7]. The effect of strain on graphene was first studied by Proctor *et al.* [8]. They performed Raman measurements on graphene on Si/SiO_2 substrates under high pressure and reported the shift rate of the in-plane phonon graphite mode (GM) frequency with pressure to be 16 $cm^{-1}\,GPa^{-1}$, significantly higher than the graphite value of 4.7 $cm^{-1}\,GPa^{-1}$ [9]. Subsequent work on graphene on various substrates (diamond [10], sapphire [10], copper [11], and SiO_2 [12]) reported a large range of shift rates from 4.0 to 10.5 $cm^{-1}\,GPa^{-1}$. It is worth noticing that for the measurements on copper, Filingtoglou *et al.* observed a sudden and irreversible change of the GM shift rates from 9.2 to 5.6 $cm^{-1}\,GPa^{-1}$ [11], the latter value being much closer to graphite. They attributed the change to the detachment of graphene from the copper substrate. Hadjikhani *et al.* also observed a shift rate of about 5 $cm^{-1}\,GPa^{-1}$ of graphene on copper [13]. Proctor *et al.* [8] initially, and Machon *et al.* [14] recently, pointed out that the GM shift rate with pressure of supported graphene is determined by the substrate via its adhesion to the graphene. Because of the difficulty of knowing the stress in graphene when it is on a substrate, we have made our measurements on unsupported graphene.

For graphite, we describe the in-plane C-C bond stretching by the Morse potential [15]:

$$E(r) = E_0[(1 - e^{-\beta(r-r_0)})^2 - 1], \tag{1}$$

where r is the separation of the nearest C-C atoms, which lie in the graphene plane, r_0 is the unstrained C-C bond length, E_0 and β denote the depth and width of the potential, respectively. The second derivative of $E(r)$ gives the force constant $k(r)$, from which we obtain the frequency $\omega(r)$ (cm^{-1}), by considering the C-C in-line antiphase vibration as an harmonic oscillation:

$$\omega(r) = \frac{1}{\pi c}\sqrt{\frac{E_0\beta^2 e^{\beta(r_0-r)}(2e^{\beta(r_0-r)} - 1)}{m}}, \tag{2}$$

where m is the mass of a carbon atom and c is the speed of light. The C-C separation r can be related to the pressure by the 2D in-plane elastic constants c_{11}^{2D} and c_{12}^{2D} ($\mathrm{N\,m}^{-1}$) [16]:

$$r(P) = r_0\left(1 - \frac{F}{c_{11}^{2D} + c_{12}^{2D}}\right), \tag{3}$$

where F is the in-plane biaxial force. It is clear that the shift rate of the GM frequency with pressure is determined by the in-plane stiffness:

$$\omega(P) = \frac{1}{\pi c}\sqrt{\frac{E_0\beta^2 e^{\frac{\beta r_0 a_{33} P}{c_{11}^{2D}+c_{12}^{2D}}}(2e^{\frac{\beta r_0 a_{33} P}{c_{11}^{2D}+c_{12}^{2D}}} - 1)}{m}}, \tag{4}$$

where a_{33} is the interlayer spacing. (This Letter involves a substantial discussion of elastic constants, which are usually labeled by c. Therefore, we use a_{33}, rather than c, to label the lattice parameter along the c axis.) These equations should apply to unsupported graphene too, except for a caveat on the choice of a_{33}. This will be discussed shortly. Proctor *et al.* attempted to make measurements on unsupported graphene, but the specimen also contained multilayer graphene and nanographite pieces [8].

To measure the thickness of one sheet of paper, one measures that of a hundred sheets and divides it by 100. Hence it is reasonable to consider the thickness of graphene as 0.34 nm, the interlayer distance in graphite [17]. This thickness can be used to obtain the values of the 2D elastic constants and the in-plane biaxial force in Eq. (3) for graphene. On the other hand, an effective thickness of graphene is sometimes introduced with an effective Young's modulus, by describing graphene as a continuum plate made of 3D isotropic material [4], for various purposes. For example, Munoz *et al.* described the ballistic thermal conduction of graphene very well by this model [18]. This approach can lead to a value of thickness as small as 0.066 nm [5]. Despite the success that these definitions bring in many cases, neither definition seems to be appropriate to define the change of thickness resulting from the out-of-plane strain of graphene.

To solve the challenge in estimating the out-of-plane stiffness, we go back to Eq. (4) for graphite. We first test how well this theoretical model describes the experimental results on graphite by Hanfland *et al.* [9]. In our previous work [19], we obtained the E_0 and β in Eq. (1) by *ab initio* calculations [20], inserted their values and the experimental values for the elastic constants c_{11} and c_{12} [21], in Eq. (4), and compared the theoretical curve for the GM frequency shift rate with pressure $\omega(P)$ to the experimental data. We found that the theoretical curve is very straight, and did not describe the large sublinearity in the experimental data. These two only agreed when we introduced an extremely small c_{33} of 39 GPa (compared to 1248 GPa of $c_{11} + c_{12}$) [21] and a relatively large shift rate of c_{33} with pressure, c'_{33} of 10 [22], to the a_{33} in Eq. (4), by $a_{33} = a_{33_0}[1 + (c'_{33}P/c_{33})]^{-(1/c'_{33})}$, where a_{33_0} is the unstrained interlayer distance of 0.34 nm. This indicates that the very soft out-of-plane stiffness of graphite, along with its relatively large shift rate with pressure, are responsible for the sublinearity in the shift of the in-plane phonon (GM) frequency of graphite with pressure. The effect of the out-of-plane stiffness on the shift of in-plane phonon frequency of graphite with pressure is summarized as follows—under hydrostatic pressure, the small out-of-plane stiffness of graphite results in a large compressive strain along the c axis. The in-plane force, the product of pressure and area (normal to the graphite, much compressed), is therefore reduced below a linear dependence on pressure. The in-plane phonon frequency, presumably shifting linearly with in-plane force, therefore shifts sublinearly with pressure. Each step can be quantified as demonstrated above. Reference [19] provides further details. We now use this approach to estimate the out-of-plane stiffness of graphene.

In this work, we apply high pressure to unsupported graphene in *N*, *N*-Dimethylformamide (DMF), measure the in-plane stiffness of graphene, and estimate the out-of-plane stiffness by its effect on the shift of the in-plane phonon frequency with pressure.

We used chemical vapor deposition (CVD) monolayer graphene grown on copper. The details of the growth method are provided in Ref. [23]. We cut the samples to 5 cm × 5 cm. The Raman spectra taken from several points on the samples all exhibit the 2D peaks at least 2 times more intense than the *G* peaks, which is the fingerprint for monolayer graphene on substrates. We observed no change of color on the graphene samples under a microscope, indicating the consistency of the number of layers over the whole sample area. The CVD graphene contains defects. Under a microscope we observed small dots of the size less than 1 μm, where monolayer graphene started to grow and grain boundaries exist where these growing monolayer single crystals met. This work focuses on the shift of the

GM frequency with pressure, which is determined by the sp^2 bond stiffness at an applied in-plane force in the size of a laser spot (about 10 μm). We think neither the bond stiffness nor the force on these bonds could be affected by those dots or the grain boundaries. Also the Raman spectra containing these defects do not present any additional peaks over the GM range. We took advantage of a wet transfer method [24] to obtain unsupported monolayer graphene in solution, as briefly described below. First, a thin poly(methyl methacrylate) (PMMA) layer was spin coated on graphene/Cu and baked. Then we removed the copper substrate in an etchant ($CuSO_4 \cdot 5H_2O$ and HCl), leaving PMMA/graphene floating on the surface of the solvent. We transferred the PMMA/graphene membrane into dimethylformamide (DMF) after rinsing the membrane in deionized water. The graphene was free-floating in DMF as the covering PMMA had been dissolved. It is known that there is no stable graphene suspension, so the free-floating transparent graphene should slowly precipitate and it is difficult to locate. In order to get a good signal from the Raman measurements, we increased the concentration of graphene by continuing to transfer PMMA/graphene membranes into DMF until saturated PMMA appeared. We gently heated the solution at 50 °C to further increase the concentration of graphene and took some of the solution from the bottom of the container, as sample *D*, graphene in DMF. We took the saturated PMMA (still covering the graphene) out of the solution as sample *P*, graphene in PMMA. We performed Raman measurements under high pressure on both samples.

We sought to obtain unsupported monolayer graphene. The free-floating monolayers may interact by van der Waals bonding to form multilayer graphene—more likely when the graphene concentration increases. We observed a single and strong 2D peak for sample *P*, having a 2D-to-*G* integrated area ratio of 1.3, similar to that of supported monolayer graphene. For sample *D*, however, the 2D peak is weaker than the *G*. It is worth noticing that many factors determine the intensity of a Raman peak and in particular the effect of having DMF (or other solutions) on both sides of a graphene layer on the intensity of its 2D peak is unknown. On the other hand, interactions between graphene layers usually increase the number of 2D peaks above the one observed for a monolayer [25]. We reasonably conclude that the interaction between the graphene pieces in sample *D* is too weak to form multilayer graphene from the objectively fitted single 2D peak by the Bayesian information criterion (BIC) [26]. The single 2D peak resulting from using the Bayesian fitting method (the value of BIC for one component is 4950.83, compared to 4964.34 for two) is consistent with our graphene remaining monolayer in solution. In addition, if one wrongly used a single peak to fit a 2D band consisting of several peaks of multilayer graphene, the fitted width would be significantly larger than the typical value for monolayer graphene. Here we obtained the peak width of about 31 cm^{-1} (see Fig. 1 in the Supplemental Material (SM) [27–32]) in the hydrostatic regime, comparable to the reported value for monolayer graphene in Ref. [25]. This is additional evidence of monolayer graphene. Moreover, multilayer formation from an initially monolayer dispersion should increase significantly the 2D width (split in fact) with respect to the GM. We observed the width of the GM and 2D peaks in our samples to both be similar to those of the monolayer graphene reported in Ref. [25] (see our Figs. 1 and 2 in the SM). This again is complementary evidence of monolayer graphene. The details are provided in the SM.

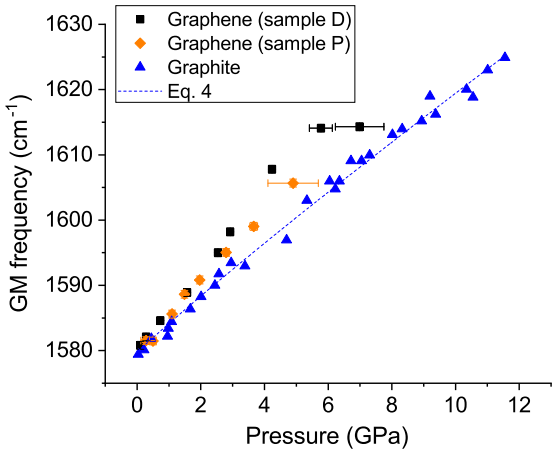

FIG. 1. The GM frequency of graphene in samples *D* (black squares) and *P* (orange diamonds) is plotted vs pressure. The data of graphite [9] (blue triangles) are also plotted with the theoretical line of Eq. (4) (blue dashed line) for comparison. The uncertainty in both pressure and frequency is plotted where it exceeds the size of a data point.

We move on to the response of unsupported graphene to pressure. We present all the GM spectra under pressure in the SM. Figure 1 shows the frequency of the in-plane phonon GM of graphene in samples *P* and *D* at various pressures, to compare with graphite data [9]. The theoretical line of Eq. (4) is also plotted and describes the graphite data very well. The uncertainty in frequency comes from the fitting and the resolution of the Raman system. It is very small and barely exceeds the size of a data point for all the graphene data. The uncertainty in pressure comes from the measurements on different ruby pieces, the larger *R*-line deviation, the higher nonhydrostaticity. We rule out the last two data points of sample *D* and the first and the last points of sample *P* in the following fitting as they are clearly not under good hydrostatic conditions. In general, unsupported graphene behaves very similarly to graphite under pressure, in terms of the shift rates of the GM, in contrast to previous published results on supported graphene.

Sample *D* contains unsupported monolayer graphene in liquid solution. We have 7 data points under reasonably good hydrostatic condition. It appears that the first 4 and the last 3 behave differently. To objectively determine it, we linear-fit all the 7 as model 1 and separately linear-fit the

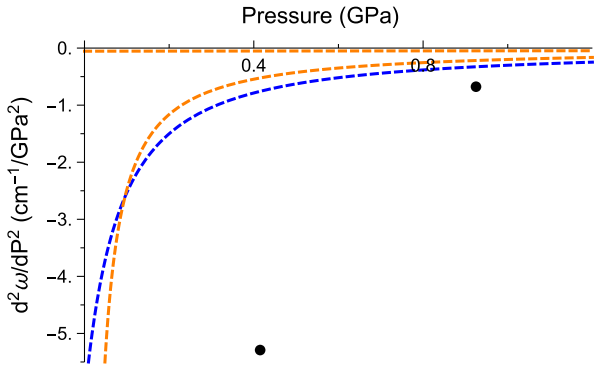

FIG. 2. The second derivative of the GM frequency to pressure (black dots) of the graphene in sample D is plotted vs pressure, with the optimal fit (blue dashed line) by the second derivative of the Eq. (4) to pressure. Two curves (orange dashed lines) by increasing or decreasing the value of c_{33} by 100 times are plotted to be compared with the optimal fit.

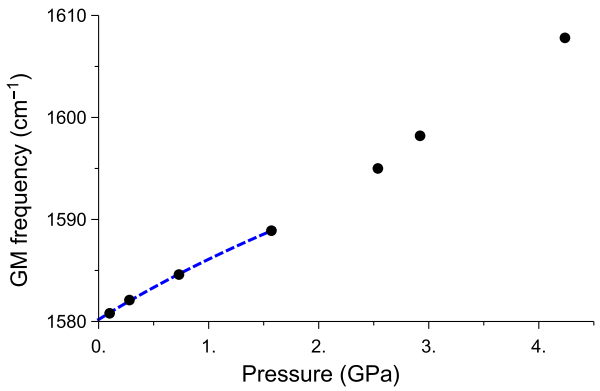

FIG. 3. The GM frequency of the graphene in sample D is plotted vs pressure. These data points, taken from Fig. 1, have a small uncertainty in pressure, implying good hydrostaticity. The optimal empirical fit of the first four points (unsupported graphene) is shown in blue dashed line.

first 4 and the last 3 as model 2. We employ the maximum likelihood estimation and compare the corrected Akaike information criterion (AIC) (used when the number of data points is small) for these two models [33], and find that the separate fit is significantly preferred by the data (21.55 vs 28.42 of AIC). It is reasonable to attribute the first 4 data points to unsupported graphene, with a slope of 5.4 $\mathrm{cm^{-1}\,GPa^{-1}}$, very close to 4.7 $\mathrm{cm^{-1}\,GPa^{-1}}$ of graphite. We think that the higher slope of the last 3 at 7.5 $\mathrm{cm^{-1}\,GPa^{-1}}$ is likely due to adhesion to the surrounding solidified DMF, similar to supported graphene on a substrate.

We now focus on the sublinearity of the GM shift with pressure. As we mentioned, the curvature is due to the large reduction of the in-plane biaxial force from the large anisotropy of graphite. We attempt to apply Eq. (4) to the first 4 points. Despite the shift rates being similar for graphite (4.7 $\mathrm{cm^{-1}\,GPa^{-1}}$) and graphene (5.4 $\mathrm{cm^{-1}\,GPa^{-1}}$), this difference is much larger than the percentage difference in the frequency at zero pressure, 1578.8 $\mathrm{cm^{-1}}$ for graphite and 1580.2 $\mathrm{cm^{-1}}$ for graphene. While in Eq. (4) the intercept ($\propto \sqrt{E_0\beta}$) and slope ($\propto \sqrt{E_0\beta}$) are determined by the same factors, the best fit of the graphene data (sample D and P) will give a lower slope than required to keep the intercept and therefore the whole fitting optimal. Consequently, c_{33} and c'_{33} can only make the fitting curve straight (by being infinitely large) to compensate the lower initial slope, and will not be able to describe the curvature. On the other hand, we have 4 data points, just more than enough to determine the second derivative of Eq. (4) to pressure, which extracts the curvature regardless of the slope. We keep the value of all the parameters the same as graphite, except c_{33} as the fitting parameter, and obtain its optimal value as 1.4 ± 295 GPa, compared to 38.7 ± 0.7 GPa of graphite [21]. Despite the large error, c_{33} is much smaller than $c_{11} + c_{12}$. We present the optimal fit of the second derivative of Eq. (4) with the data in Fig. 2. Alternatively, since we know that the curvature is determined by the out-of-plane stiffness ($a_{33} = a_{33_0}[1 + (c'_{33}P/c_{33})]^{-(1/c'_{33})}$), we can empirically fit the data of graphite and graphene by $\omega = \omega_0(\delta P + 1)^{\delta'}$ with $\delta' \propto 1/c'_{33}$ and $\delta'\delta \propto 1/c_{33}$. From the optimal fit, δ' is 0.054 ± 0.01 for graphite and 0.014 ± 0.006 for graphene. $\delta'\delta$ is $(3.2 \pm 1.4) \times 10^{-3}$ $\mathrm{GPa^{-1}}$ for graphite and $(4.3 \pm 3.9) \times 10^{-3}$ $\mathrm{GPa^{-1}}$ for graphene. We present all the data points at the hydrostatic condition of sample D and the optimal empirical fit of the first 4 points in Fig. 3. The results suggest that unsupported graphene in solution presents a similar out-of-plane stiffness to graphite, as expected. We can also obtain the initial shift rate of the GM with pressure as $((6.7 \pm 0.6)$ GPa in DMF.

The PMMA used in this study is a gel. The adhesion of the gel to graphene is unclear. We use sample P to compare with sample D and therefore we apply the same empirical fitting as before to the data over a similar pressure range, after ruling out those at nonhydrostatic conditions.

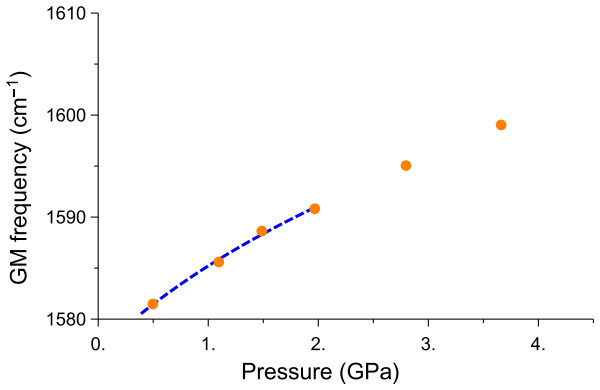

FIG. 4. The GM frequency of the graphene in sample P is plotted vs pressure. These data points, taken from Fig. 1, have only small uncertainties in pressure, implying good hydrostaticity. The fit of the first four points over the similar range to the fit in Fig. 3 is shown as a blue dashed line.

The slope is similar to sample D (see Fig. 1, initial shift rate of (10.4 ± 5.2) GPa) and the fitting results for the curvature are similar, giving δ' of 0.013 ± 0.01 and $\delta'\delta$ of 6.6 ± 14.8 GPa^{-1}. This indicates that the gel, like a liquid, and unlike solid substrates, has little adhesion to graphene under pressure. Then we can consider the graphene in sample P as "unsupported" and it again shows a similar in-plane and out-of-plane stiffness to graphite. We present the data and corresponding fit in Fig. 4.

In conclusion, we have defined 3D strain in 2D graphene by recognizing that it is the electron orbitals that react to strain. In particular, it is the p orbitals above and below the hexagonal network of sp^2 bonded carbon atoms that resist compression along the c axis. Thus the elastic constant c_{33} is defined by the resistance of the p orbitals to compression. We have performed Raman measurements on unsupported graphene in DMF and PMMA under pressure. We find that the shift rate of the in-plane phonon GM frequency of graphene (5.4 cm^{-1} GPa^{-1}) with pressure is close to that of graphite (4.7 cm^{-1} GPa^{-1}), indicating a similar in-plane stiffness and anharmonicity of graphene to graphite, in contrast to previous high-pressure measurements on supported graphene (16 cm^{-1} GPa^{-1}), if the graphene has not coagulated to graphite, and we do not believe it has from the evidence presented. The small out-of-plane stiffness of graphite results in a reduction of the in-plane force under pressure, and therefore the GM frequency shifts sublinearly with pressure. We estimate a similar out-of-plane stiffness for graphene (1.4 ± 295 GPa) to graphite (38.7 ± 0.7 GPa) from this effect and we consider that this is a reliable and meaningful way to estimate the out-of-plane strain and stiffness for 2D materials, as it corresponds to real experimental observables and does not involve an ambiguously defined, physically meaningless effective thickness. This method applies not only to graphene and graphite, but also to other 2D materials and their 3D forms.

The authors are grateful for valuable comments on the interpretation of the results by Dr. D. Holec from Montanuniversitat Leoben and Professor A. San Miguel from Univerité Lyon 1.

Y. W. Sun and W. Liu contributed equally to this work.

*yiwei.sun@qmul.ac.uk
†d.dunstan@qmul.ac.uk
‡c.humphreys@qmul.ac.uk

[1] K. S. Novoselov, A. K. Geim, S. V. Morozov, D. Jiang, Y. Zhang, S. V. Dubonos, I. V. Grigorieva, and A. A. Firsov, Science **306**, 666 (2004).
[2] M. Kawaguchi, S. Kuroda, and Y. Muramatsu, J. Phys. Chem. Solids **69**, 1171 (2008).
[3] P. R. Bonneau, J. B. Wiley, R. B. Kaner, and M. F. Mansuktto, Inorganic Syntheses **30**, 33 (1995).
[4] B. I. Yakobson, C. J. Brabec, and J. Bernholc, Phys. Rev. Lett. **76**, 2511 (1996).
[5] L. Wang, Q. Zheng, J. Z. Liu, and Q. Jiang, Phys. Rev. Lett. **95**, 105501 (2005).
[6] R. J. Young, I. A. Kinloch, L. Gong, and K. S. Novoselov, Compos. Sci. Technol. **72**, 1459 (2012).
[7] N. C. Yeh, C.-C. Hsu, M. L. Teague, J.-Q. Wang, D. A. Boyd, and C.-C. Chen, Acta Mech. Sin. **32**, 497 (2016).
[8] J. E. Proctor, E. Gregoryanz, K. S. Novoselov, M. Lotya, J. N. Coleman, and M. P. Halsall, Phys. Rev. B **80**, 073408 (2009).
[9] M. Hanfland, H. Beister, and K. Syassen, Phys. Rev. B **39**, 12598 (1989).
[10] C. Bousige, F. Balima, D. Machon, G. S. Pinheiro, A. Torres-Dias, J. Nicolle, D. Kalita, N. Bendiab, L. Marty, V. Bouchiat, G. Montagnac, A. G. Souza Filho, P. Poncharal, and A. San-Miguel, Nano Lett. **17**, 21 (2017).
[11] K. Filintoglou, N. Papadopoulos, J. Arvanitidis, D. Christofilos, O. Frank, M. Kalbac, J. Parthenios, G. Kalosakas, C. Galiotis, and K. Papagelis, Phys. Rev. B **88**, 045418 (2013).
[12] J. Nicolle, D. Machon, P. Poncharal, O. Pierre-Louis, and A. San-Miguel, Nano Lett. **11**, 3564 (2011).
[13] A. Hadjikhani, J. Chen, S. Das, and W. Choi, *Suppl. Proc.: Vol.2: Materials Properties, Characterization and Modeling, TMS (The Minerals, Metals & Materials Society)* (John Wiley & Sons, Hoboken, New Jersey, 2012), pp. 78–79.
[14] D. Machon, C. Bousige, R. Alencar, A. Torres-Dias, F. Balima, J. Nicolle, G. S. Pinheiro, A. G. Souza Filho, and A. San-Miguel, J. Raman Spectrosc. **49**, 121 (2018).
[15] P. M. Morse, Phys. Rev. **34**, 57 (1929).
[16] G. Savini, Y. J. Dappe, S. Öberg, J.-C. Charlier, M. I. Katsnelson, and A. Fasolino, Carbon **49**, 62 (2011).
[17] P. Trucano and R. Chen, Nature (London) **258**, 136 (1975).
[18] E. Munoz, J. Lu, and B. I. Yakobson, Nano Lett. **10**, 1652 (2010).
[19] Y. W. Sun, D. J. Dunstan, M. A. Hartmann, and D. Holec, Proc. Appl. Math. Mech. **13**, 7 (2013).
[20] D. Holec, M. A. Hartmann, F. D. Fischer, F. G. Rammerstorfer, P. H. Mayrhofer, and O. Paris, Phys. Rev. B **81**, 235403 (2010).
[21] A. Bosak, M. Krisch, M. Mohr, J. Maultzsch, and C. Thomsen, Phys. Rev. B **75**, 153408 (2007).
[22] W. B. Gauster and I. J. Fritz, J. Appl. Phys. **45**, 3309 (1974).
[23] P. R. Whelan, D. Huang, D. Mackenzie, S. A. Messina, Z. Li, X. Li, Y. Li, T. J. Booth, P. U. Jepsen, H. Shi, and P. Bøggild, Opt. Express **26**, 17748 (2018).
[24] A. C. Ferrari, J. C. Meyer, V. Scardaci, C. Casiraghi, M. Lazzeri, F. Mauri, S. Piscanec, D. Jiang, K. S. Novoselov, S. Roth, and A. K. Geim, Science **324**, 1312 (2009).
[25] A. C. Ferrari *et al.*, Phys. Rev. Lett. **97**, 187401 (2006).
[26] G. E. Schwarz, Ann. Stat. **6**, 461 (1978).
[27] See Supplemental Material at http://link.aps.org/supplemental/10.1103/PhysRevLett.123.135501 for the experimental details of the Raman measurements under high pressure and the evidence of unsupported monolayer graphene, which includes Refs. [28–32].
[28] H. K. Mao, J. Xu, and P. M. Bell, J. Geophys. Res. **91**, 4673 (1986).
[29] A. Kumar, W. Escoffier, J. M. Poumirol, C. Faugeras, D. P. Arovas, M. M. Fogler, F. Guinea, S. Roche, M. Goiran, and B. Raquet, Phys. Rev. Lett. **107**, 126806 (2011).

[30] J. Gonzalez, R. Valiente, and F. Rodriguez, Joint AIRAPT-25th and EHPRG-53rd conference, oral contribution [029].
[31] C. Neumann, S. Reichardt, P. Venezuela, M. Drögeler, L. Banszerus, M. Schmitz, K. Watanabe, T. Taniguchi, F. Mauri, B. Beschoten, S. V. Rotkin, and C. Stampfer, Nat. Commun. **6**, 8429 (2015).
[32] P. Ratajczyk, S. Sobczak, and A. Katrusiak, Cryst. Growth Des. **19**, 896 (2019).
[33] J. E. Cavanaugh, Stat. Probab. Lett. **33**, 201 (1997).